PHYSICAL REVIEW B
CONDENSED MATTER

THIRD SERIES, VOLUME 45, NUMBER 19 15 MAY 1992-I

Electronic structure, cohesive properties, and phase stability of Ni_3V, Co_3V, and Fe_3V

W. Lin, Jian-hua Xu, and A. J. Freeman
Department of Physics and Astronomy, Northwestern University, Evanston, Illinois 60208-3112
(Received 22 February 1991)

The electronic structure and cohesive properties (including equilibrium lattice constants, bulk modulus, and formation energy) of the intermetallic compounds Ni_3V, Co_3V, and Fe_3V in their $L1_2$, $D0_{22}$, and $D0_{19}$ structures have been determined by means of the self-consistent total-energy linear-muffin-tin-orbital method based on the local-density approximation. The correct phase preference and stability of these compounds are obtained; the rigid-band approximation is found to hold well for describing the electronic structure of these compounds having the same crystal structure. The correlation between the ordered structure and the semiempirical rule of Liu on the number of valence electrons per atom is shown to be associated with the filling up of the bonding states in a specific structure.

I. INTRODUCTION

Because of their attractive mechanical, electrical, and magnetic properties, intermetallic compounds have a wide range of applications in different areas and have generated many interesting questions for researchers.[1,2] Specifically, the structurally ordered intermetallic compounds such as TiAl, Ti_3Al, NiAl, Ni_3Al, and Ni_3V have been found to possess desirable high yield strength at high temperatures, which makes them extremely attractive for potential applications as aerospace materials.[3] The high strength of Ni_3V is believed to be due to its ordered structure and strong bonding character.[4] However, the severe brittleness of these compounds remains an obstacle to the application of these compounds. According to von Mises's criterion,[5] it is possible to form a uniform deformation only if a structure has more than five independent slip systems. It is believed that the lack of slip systems in Ni_3V is a major cause of its brittleness[4] since it crystallizes into the low-symmetry tetragonal $D0_{22}$ crystal structure. In A_3B-like compounds, the highly symmetric cubic $L1_2$ structure is the most desirable from the point of view of generating enough slip systems.

It was found recently[4,6] that by adding Co and Fe to Ni_3V, the pseudobinary compound $(Ni,Co,Fe)_3V$ has the following properties: (i) it can be stabilized in the cubic $L1_2$ structure at ambient temperature in a long-range-ordered way; (ii) its structural stability can be correlated to the e/atom (valence electrons per atom) ratio; and (iii) it crystallizes in the $L1_2$ structure only when $e/a\text{tom} < 7.89$. Since Co and Fe have lower e/atom than Ni, the addition of Co and Fe to Ni_3V can lower the overall e/atom to an appropriate value, in which the cubic $L1_2$ structure will be favorable. When $e/a\text{tom} > 8.54$, the compound forms in the tetragonal ($D0_{22}$) structure. For e/atom between 7.89 and 8.54, it forms a complicated transitional structure composed of a mixture of the cubic and hexagonal structures. The apparent dominant role of the e/atom value in determining phase preference and phase transition in these pseudobinary compounds has attracted much attention. Recently, the correct phase preference between the $L1_2$ and $D0_{22}$ structures of Ni_3V and Co_3Ti has been reported,[7] and it is found that when e/atom is greater than 8.65, the $D0_{22}$ phase is more stable than the $L1_2$ phase.

In this paper we report electronic structures and cohesive properties of Ni_3V, Co_3V, and Fe_3V in their $L1_2$, $D0_{22}$, and $D0_{19}$ phases. Their observed phase preference and stability are confirmed theoretically, i.e., Ni_3V in the $D0_{22}$ structure and Co_3V in the $L1_2$ structure have the lowest total energy among the three different structures considered. On the other hand, exceptionally small formation energies for Fe_3V in any of the three structures studied imply that Fe_3V favors a (disordered) homogeneous solid solution rather than an ordered structure.

The calculated lattice constants $a = 3.53$ Å and $c/a = 2.031$ for $D0_{22}$ Ni_3V and $a = 4.98$ Å for $D0_{19}$ Co_3V are in reasonable agreement with experiment [$a = 3.5424$ Å and $c/a = 2.036$ (for $D0_{22}$ Ni_3V) and $a = 5.032$ Å (for a hexagonal κ phase Co_3V), respectively]. To our knowledge, no experimental heat of formation is available for Ni_3V, however the calculated formation energy 23.1 kcal/mol for Ni_3V is comparable with that for isostructural compounds Ni_3Ti and Ni_3Nb (33.5 ± 1.5 and 30.4 kcal/mol). Furthermore, we found that the rigid band scheme holds well for describing the electronic structures

of Fe_3V, Co_3V, and Ni_3V in the same structure. Therefore, we employed the "pseudocharge" scheme based on the rigid band concept to study the empirical correlation between the structural stability and the electron concentration e/atom for the pseudobinary compounds $(Ni,Co,Fe)_3V$, and found that the e/atom is associated with the filling up of the bonding states in a specific structure.

II. COMPUTATIONAL DETAILS

The relative structural stability among the three ($L1_2$, $D0_{22}$, and $D0_{19}$) different structures was studied by a total-energy approach based on the local-density approximation (LDA),[8] namely the self-consistent linear-muffin-tin-orbital (LMTO) method including the combined correction term in the atomic-sphere approximation (ASA).[9] The von Barth–Hedin formula[10] is used for the exchange-correlation potential. For simplicity, we assume the elements to have the same Wigner-Seitz (WS) radius. We include basis sets up to $l=2$ (i.e., d orbital) and treat the core electrons fully relativistically and the valence electrons semirelativistically (i.e., neglecting spin-orbit coupling). The total energies were calculated for varying lattice constants (i.e., WS radius) in order to locate the equilibrium lattice constant. The calculations are considered to be converged when the deviation between the input and output potential is less than 0.1 mRy. It has been known that the total energy E depends upon $n_k^{-2/3}$ (cf. Ref. 11), where n_k is the number of k points within the irreducible wedge of the Brillouin zone (IBZ). Thus we can obtain an extrapolated total energy for an infinite number of k points from the total energy calculated using a finite number of k points within the IBZ in order to eliminate possible errors caused by an insufficient number of sampling k points.[12] Since the total energies for the pure metal were treated in the same way, the formation energy is obtained by subtracting the weighted sum of total energies of the constituent elements from the total energy of the compound [i.e., $\Delta E=E_{M_aN_b}-(aE_M+bE_N)$ (Ref. 13)]. Hence ΔE represents the released energy when the compound is formed, which relates to the stability of the compounds. A parabolic fitting was adopted to obtain the bulk modulus. Since the bulk modulus was calculated from the second derivative of the total energy versus the volume of the unit cell, a 10–30% error is generally involved.[11]

The $L1_2$, $D0_{22}$, and $D0_{19}$ phases are close-packed structures. The $L1_2$ is a fcc-like structure with corners and face centers occupied by V and Ni (or Co,Fe) atoms, respectively. For comparison with the $D0_{22}$ structure, a double-sized $L1_2$ cell is presented in Fig. 1(a). Figure 1(b) represents tetragonal $D0_{22}$, which only differs from $L1_2$ by shifting the atomic position along the [110] direction by $(a/2)(1,1,0)$ on the middle plane. Therefore, we can distinguish the two inequivalent Ni sites labeled as site A and site B according to their local environment. The $D0_{19}$ structure [cf. Fig. 1(c)] is a hexagonal structure. On the top and bottom planes the atoms occupy corners, face centers, and edge centers, and on the middle plane the

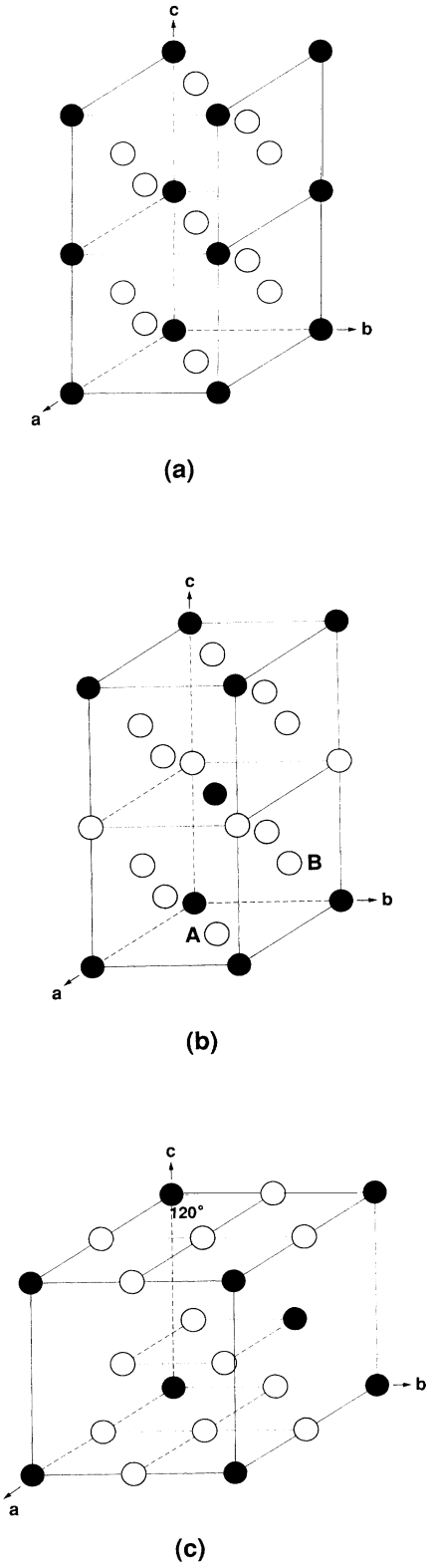

FIG. 1. Unit cell for (a) the $L1_2$ structure (two unit cells); (b) the $D0_{22}$ structure, where A and B represent two inequivalent sites of the same atoms; and (c) the $D0_{19}$ structure, where the angle between axes a and b is 120°. a, b, and c label the three axes of the unit cell. Filled and empty circles represent M (M = Ni,Co,Fe) and V atoms, respectively.

atoms are located at the (1/3,1/6,1/2) and equivalent positions. Each plane contains three Ni or (Co,Fe) atoms and one V atom. The c/a value is fixed at the ideal close-packed value 0.816 for $D0_{19}$ and 2.0 for $D0_{22}$ structures, except for the Ni_3V case, where the c/a of the $D0_{22}$ structure was relaxed to obtain a minimum energy.

III. RESULTS AND DISCUSSION

A. Cohesive properties, electronic structures, and phase stabilities of Ni_3V, Co_3V, and Fe_3V

1. Ni_3V

The total energy vs WS radius is shown in Fig. 2(a). The difference in the equilibrium WS radii, r^0_{WS}, between any two of these three structures is found to be within 1%. Therefore, the atomic volume for the different structures is nearly constant. In agreement with experiment and Ref. 15, the $D0_{22}$ structure has the lowest total energy among these three structures [cf. Fig. 2(a)]. The relative stability—$D0_{22}$, $D0_{19}$ to $L1_2$—remains the same as found in Ref. 15. The calculated equilibrium cohesive properties are presented in Table I. The calculated lattice constants $a=3.53$ Å and $c/a=2.031$ are in good agreement with both experiment [$a=3.5424$ Å and $c/a=2.036$ (Ref. 14)] and Ref. 15 (cf. Table I). However, due to the combined correction term being taken into account in these calculations, the equilibrium constants are slightly smaller (0.01 Å) than previously calculated[15] for the $D0_{22}$ and $D0_{19}$ structures. On the other hand, the formation energies and the bulk moduli are generally 20–30% larger than those of Refs. 15—with the $D0_{22}$ structure having the largest formation energy (23.1 kcal/mol), which can be compared with that of isostructural compounds Ni_3Ti and Ni_3Nb (33.5 ± 1.5 and 30.4 kcal/mol),[16] because no experimental data on the formation energy for Ni_3V are available.

In order to understand the phase stability from the microscopic point of view, we inspect the density of states (DOS) of Ni_3V (cf. Fig. 3). As found before,[15] it can be seen from the partial density of states that a strong hybridization between the Ni d and V d state dominates the cohesion (i.e., the structural stability). In the $L1_2$ (paramagnetic) case [cf. Fig. 3(a)], a well-separated bonding and antibonding region caused by the d-d hybridization creates a pseudogap at about 0.5 eV below E_F; the main d-d peak is located at about 2.3 eV below the Fermi level. Note that the E_F resides right on the peak in the antibonding region, resulting in a high value of $N(E_F)$ ($\sim$17.1 states/eV f.u.). This implies a strong (magnetic) instability for the paramagnetic $L1_2$ phase. In fact, the onset of ferromagnetism serves to reduce the value of $N(E_F)$ quite dramatically to 7.3 states/eV f.u., with the spin-down peak shifted to a position located higher in energy than E_F. However, the Fermi level still lies on the peak of the spin-up part [cf. Fig. 3(d)]. Similar to the $L1_2$ case, the Fermi level for the $D0_{19}$ phase [cf. Fig. 3(b)] lies on the shoulder of a peak in the antibonding region. On the other hand, the location of E_F for $D0_{22}$ is shifted to-

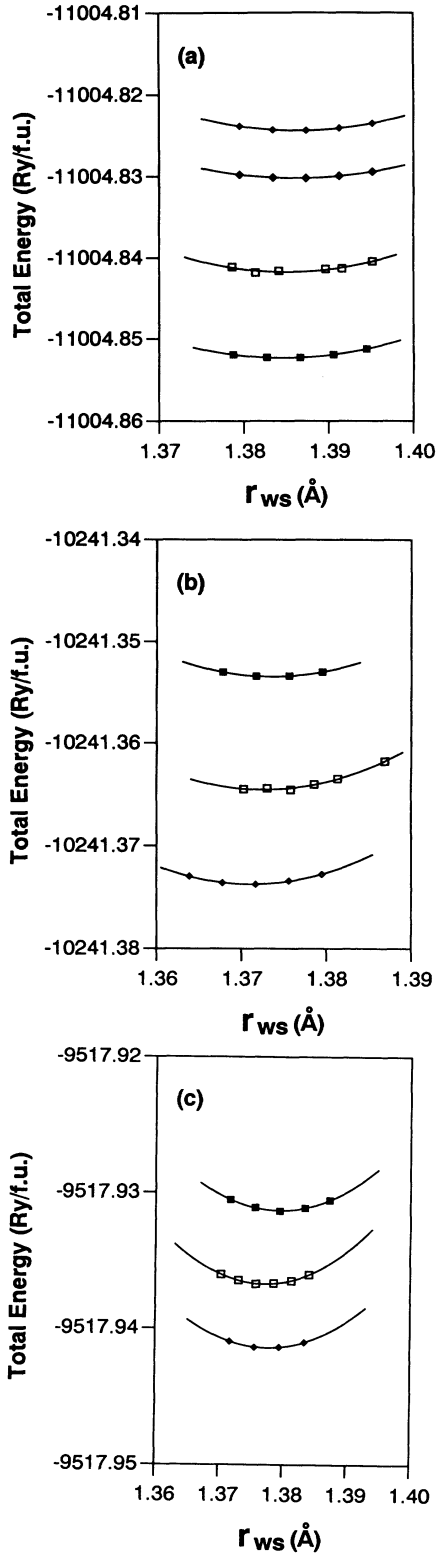

FIG. 2. Total energy (Ry/f.u.) vs Wigner-Seitz radius r_{WS} (Å) for the $L1_2$, $D0_{19}$, and $D0_{22}$ structures, obtained using 30 k points in the IBZ. (a) Ni_3V, filled rhombus, empty rhombus, empty square, and filled square stand for the $L1_2$ (paramagnetic state), $L1_2$ (ferromagnetic state), $D0_{19}$, and $D0_{22}$ structures, respectively. (b) Co_3V and (c) Fe_3V, filled rhombus, empty square, and filled square stand for the $L1_2$, $D0_{19}$, and $D0_{22}$ structures, respectively.

TABLE I. The calculated equilibrium cohesive properties (lattice constant a, WS radius r_{WS}^0, bulk modulus B, and formation energy ΔE) and DOS at E_F of Ni_3V in the $L1_2$, $D0_{19}$, and $D0_{22}$ structures.

	Ni_3V		a (Å)	r_{WS}^0 (Å)	B (Mbar)	ΔE (kcal/mol)	DOS at E_F (states/eV f.u.)
Calc.	$L1_2$ (paramagnetic)		3.55	1.387	2.5	13.1	17.1
	$L1_2$ (ferromagnetic)		3.55	1.387	2.5	14.9	7.3
	$D0_{19}$		5.00 ($c/a=0.816$)	1.381	2.7	18.4	4.5
	$D0_{22}$	this work	3.53 ($c/a=2.031$)	1.387	2.5	23.1	3.2
		a	3.54 ($c/a=2.036$)	1.392	2.3	21.3	2.68
		b	3.522 ($c/a=2.04$)		2.59		
Expt.[c]	$D0_{22}$		3.5424($c/a=2.036$)	1.393			

[a]Reference 15.
[b]Reference 7.
[c]Reference 14.

wards high binding energy by about 0.4 eV with respect to that of the $L1_2$ phase; in other words, the centroid of the band for the $D0_{22}$ phase [cf. Fig. 3(c)] is shifted downward as compared with the $L1_2$ phase. This implies that for the $D0_{22}$ phase the valence electrons are more efficiently packed into the bonding region (according to the covalent approach,[17] this means maximizing the bonding effect), resulting in a stronger structural stability compared with the other two phases. Moreover, it is interesting to note that the density of states at the Fermi level is found to be inversely related to the formation energy (i.e., the structural stability);[15,18] the energetically favored $D0_{22}$ has the lowest $N(E_F)$ (3.2 states/eV f.u.).

2. Co_3V

The total energy vs WS radius is plotted in Fig. 2(b). Similar to the Ni_3V case, the atomic volume for the different structures is nearly invariant; the deviation of r_{WS}^0 from one structure to another is negligible. However, for the relative structural stability of Co_3V, we found, contrary to the case of Ni_3V, the ordering $L1_2$, $D0_{19}$, to $D0_{22}$. The cubic $L1_2$ structure is the most stable structure among the three structures, which is consistent with experiment. It was reported[19,20] that Co_3V exists naturally in two phases [a low-temperature ordered hexagonal structure, known as the κ or Al_3Pu-type phase, and an $L1_2$ (or Cu_3Au) -type phase in the vicinity of 1070 °C] in the composition range up to 40 at. % V. Both phases are closely related to the ordered cubic $L1_2$ structure and can be viewed as a mixture of the different stacking order and stacking period of the close-packed ordered layer of Co_3V. For instance, the κ phase has a stacking order that can be considered as a mixture of 33.3% hexagonal and 66.7% cubic and has the six-layer period of the close-packed ordered layers of Co_3V. The calculated cohesive properties for Co_3V are listed in Table II. The lattice constant of the $D0_{19}$ phase ($a=4.98$ Å) is consistent with the experimental data ($a=5.03$ Å) (Ref. 21) for the κ phase; unfortunately, no experimental lattice constant is available for the cubic $L1_2$ phase. The formation energy of Co_3V in the $L1_2$ phase is comparable with that of Ni_3V.

The DOS of Co_3V in the three structures, as shown in Fig. 4, may help to elucidate the structural stability of Co_3V. It is interesting to note that there is a significant overall resemblance of the DOS between the $L1_2$ and $D0_{19}$ structures [cf. Figs. 4(a) and 4(b)], and that the Fermi levels (measured from the bottom of the band) lie at nearly the same position—in a valley in the bonding region for these two phases.

On the other hand, note that there is a markedly different feature of the DOS between the cubic $L1_2$ (or the hexagonal $D0_{19}$) and the tetragonal $D0_{22}$ phases [cf. Fig. 4(c)]. In the former case, there is a clear pseudogap located at about 0.5–0.6 eV above E_F, which separates the bonding (between −9.0 and 0.5–0.6 eV) and the antibonding (above 0.5–0.6 eV) regions; a main d-d peak is

TABLE II. The calculated equilibrium cohesive properties (lattice constant a, WS radius r_{WS}^0, bulk modulus B, and formation energy ΔE) and DOS at E_F of Co_3V in the $L1_2$, $D0_{22}$, and $D0_{19}$ structures.

	Co_3V	a (Å)	r_{WS}^0 (Å)	B (Mbar)	ΔE (kcal/mol)	DOS at E_F (states/eV f.u.)
Calc.	$L1_2$	3.51	1.372	3.0	19.8	3.1
	$D0_{22}$	3.51 ($c/a=2.0$)	1.372	2.8	12.9	5.6
	$D0_{19}$	4.98 ($c/a=0.816$)	1.376	3.4	16.5	3.4
Expt.[a]	$hp24$ ($p\bar{6}m2$)	5.032 ($c/a=2.4384$)	1.388			

[a]Reference 14.

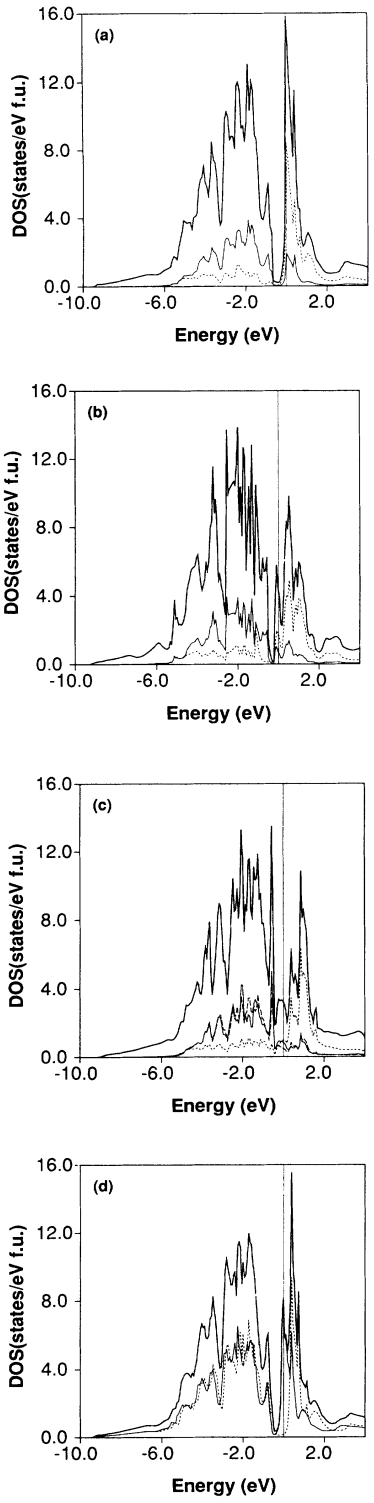

FIG. 3. Total DOS (in states/eV f.u.) and partial d DOS (in states/eV atom) for Ni_3V in the (a) $L1_2$, (b) $D0_{19}$, (c) $D0_{22}$, and (d) $L1_2$ (ferromagnetic state) structures. The thick solid line denotes the total DOS. In (a) and (b), the thin solid and the dotted lines represent the Ni d and V d states, respectively; in (c) the thin solid, the broken, and the dotted lines represent the Ni d states at site A and site B [cf. Fig. 1(c)] and the V d states, respectively. In (d) the thin solid and the dotted lines represent the total DOS for spin-up and spin-down electrons, respectively. The Fermi energy is taken as the energy zero.

located at about 1.5 eV below E_F. Now, according to the Gelatt, Williams, and Moruzzi[22] conceptual picture of the bonding character in the ordered transition-metal and non-transition-metal compounds, occupying the bonding states increases the bonding strength. Therefore, for the $L1_2$ (or $D0_{19}$) phase the valence electrons have occupied most of the bonding states; this causes the Fermi level to reside in a valley in the bonding region, and results in a lower $N(E_F)$ (3.1 and 3.4 states/eV for the $L1_2$ and $D0_{19}$ phase, respectively). This implies that in addition to their similar DOS, $D0_{19}$ and $L1_2$ have comparable stability. Thus the hexagonal $D0_{19}$ phase may be mixed with the

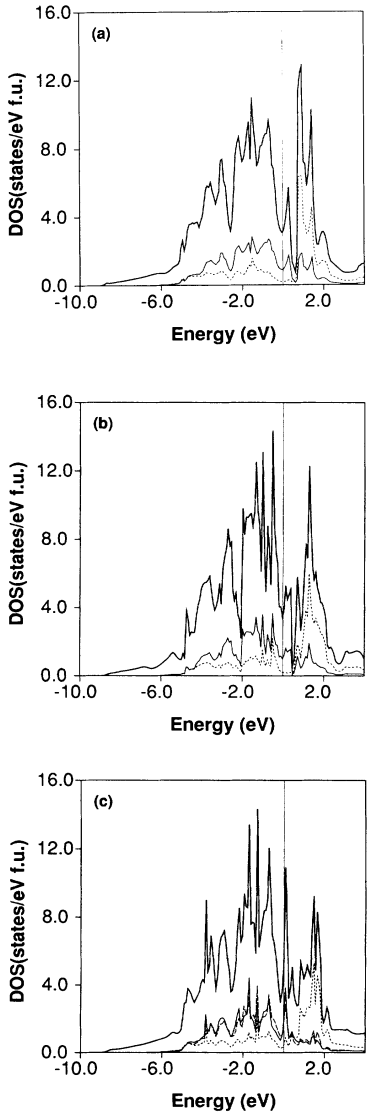

FIG. 4. Total DOS (in states/eV f.u.) and partial d DOS (in states/eV atom) for Co_3V in the (a) $L1_2$, (b) $D0_{19}$, and (c) $D0_{22}$ structures. The thick solid line denotes the total DOS. In (a) and (b), the thin solid and the dotted lines represent the Co d and V d states, respectively; in (c), the thin solid, the broken, and the dotted lines represent the Co d states at site A and site B [cf. Fig. 1(c)] and the V d states, respectively.

cubic $L1_2$ phase and cause a hybridized final phase (i.e., the Al_3Pu structure).

By contrast, for the $D0_{22}$ phase the d-d bonding region stretches from -9.0 to 0.6 eV. There is only a comparatively shallow valley in the DOS located at about 0.6 eV, which separates the bonding and antibonding region. The position of the main d-d peak has not been altered from one structure to another, but the Fermi level for the $D0_{22}$ phase resides at a rapidly ascending part of the DOS. This results in a relatively higher $N(E_F)$ (5.6 states/eV f.u.) with respect to the $L1_2$ (or $D0_{19}$) phase and is considered to be responsible for the instability of the $D0_{22}$ phase. Note that again we have an inverse relationship between $N(E_F)$ and the phase stability. In addition, Co_3V in its stable $L1_2$ (or $D0_{19}$) form having a low $N(E_F)$ is consistent with the experimental observation—alloys containing 24.2–30.1 at. % V are paramagnetic down to 4.2 K.[23]

3. Fe_3V

The total energy vs WS radius is plotted in Fig. 2(c). Similar to the other two cases, the deviation of r^0_{WS} from one structure to the other is negligible; again, the constancy of the atomic volume for the different structures is seen. Moreover, we have the same relative order of the structural stability for Fe_3V as for Co_3V, but the energy difference between any two of these three phases is much smaller than that of other two (Ni_3V or Co_3V) compounds; it is only about 5 mRy/f.u. (or 1.2 mRy/atom). Such a small energy difference between any two phases implies that Fe_3V may have a very strong probability to be found in any of these three structures. Further, the exceptionally small formation energies for Fe_3V in the three structures (cf. Table III) indicates that it may not prefer to be an ordered structure. Indeed, it is found that no ordered phase exists in nature in the region up to about 30 at. % V (Ref. 24)—only a homogeneous solid solution exists.

If we inspect the electronic structures of Fe_3V in the three structures we immediately find an interesting feature in the DOS [cf. Figs. 5(a)–5(c)], i.e., the overall resemblance of the DOS and virtually the same location (~ 8.6 eV measured from the bottom of the band) of the Fermi level for all these phases. As shown in Fig. 5, for each of them the DOS curve can be divided into bonding (between -8.5 and 0.5 eV) and antibonding (above 0.5 eV) regions, and a main d-d bonding peak located at about -1.0 eV. This means that the occupied portion of the bonding states is nearly the same (i.e., having the same extent of the band filling) for these three structures, which is consistent with a nearly invariant formation energy for these three phases (cf. Table III).

4. Discussion

Before going into the study of the pseudobinary $(Ni,Co,Fe)_3V$ compounds two remarks need to be made at this point.

(i) The pervasive hybridization between M d (M = Ni, Co, or Fe) and V d states dominates the cohesion (therefore, the structural stability) of the compounds. Due to this hybridization, their entire electronic spectra can be divided into bonding and antibonding regions, and a pseudogap resides in between. However, from the partial density of states it can be seen that the M d character is found dominantly in the region below E_F while the V d is above E_F; therefore, the V valence electrons are in general transferred onto the M sites, which agrees with electronegativity considerations. The charge transfer for the Ni_3V and Co_3V in their stable forms are presented in Table IV. Note that it is not only the electrons at the V sites that transfer onto the Ni (or Co) sites to fill up their hole states in the d bands, but there is also a charge transfer between the s states and the d states. The number of d electrons increases and the number of s electrons

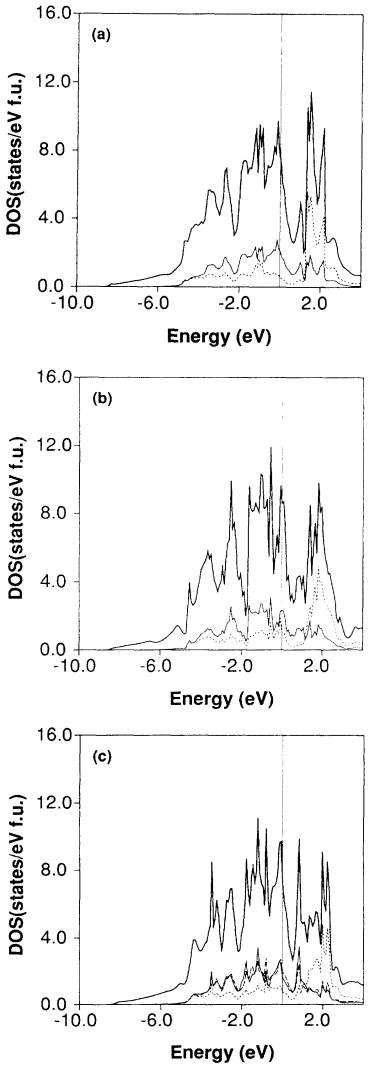

FIG. 5. Total DOS (in states/eV f.u.) and partial d DOS (in states/eV atom) for Fe_3V in the (a) $L1_2$, (b) $D0_{19}$, and (c) $D0_{22}$ structures. The thick solid line denotes the total DOS. In (a) and (b), the thin solid and the dotted lines represent the Fe d and V d states, respectively; in (c), the thin solid, the broken, and the dotted lines represent the Fe d states at site A and site B [cf. Fig. 1(c)] and the V d states, respectively.

TABLE III. The calculated equilibrium cohesive properties (lattice constant a, WS radius r_{WS}^0, bulk modulus B, and formation energy ΔE) and DOS at E_F of Fe_3V in the $L1_2$, $D0_{22}$, and $D0_{19}$ structures.

Fe_3V (Calc.)	a (Å)	r_{WS}^0 (Å)	B (Mbar)	ΔE (kcal/mol)	DOS at E_F (states/eV f.u.)
$L1_2$	3.53	1.380	2.6	6.6	7.6
$D0_{22}$	3.53 ($c/a=2.0$)	1.380	2.7	4.3	7.3
$D0_{19}$	4.98 ($c/a=0.816$)	1.376	3.1	4.6	8.2

decreases.

(ii) The general features of the DOS for these three compounds in the same structure resemble each other. For instance, if the bottom of the band for Fe_3V and Ni_3V in the $L1_2$ structure is shifted to coincide with that of Co_3V in the $L1_2$ structure, the three DOS curves nearly fall onto the same contour (cf. Fig. 6). In other words, the rigid band holds well for representing the electronic structures of Fe_3V, Co_3V, and Ni_3V in the same type of crystal structure. It is indeed seen that the structural stability of the $L1_2$ structure increases from Fe_3V to Co_3V because Co_3V has more valence electrons (therefore, the larger the occupied portion of the bonding states) than that of Fe_3V. Now with an increase of the number of valence electrons from Co_3V to Ni_3V, the valence electrons occupy states up to the antibonding region in Ni_3V leading to a phase transition to the $D0_{22}$ structure.

B. Structural stability vs e/atom in pseudobinary $(Ni,Co,Fe)_3V$ compounds

Based upon the arguments stated above, we presume that the electronic structure for the pseudobinary compounds $(Ni,Co,Fe)_3V$ can be interpreted in terms of the rigid band scheme and used with a fictitious "pseudocharge" on the Ni (or Co,Fe) sites. The different atomic percentage substitutions of Ni (or Co,Fe) (i.e., different e/atom) in the M sites of M_3V compounds (M=Ni, Co, or Fe) can be simply realized by changing the pseudocharge on the M sites uniformly, and a linear dependence between the lattice constants and the concentration (Vegard's law[25]) was assumed.

We calculated the total energy vs the electron concentration for the pseudobinary compound $(Fe,Co,Ni)_3V$ in the three ($L1_2$, $D0_{19}$, and $D0_{22}$) different phases. With the total energy of the $D0_{19}$ phase as a reference energy, the dependence of the total energy of the $L1_2$ (or $D0_{22}$) phase on the electron concentration (e/atom) is plotted in Fig. 7. It can be clearly seen that it can be divided, according to the phase stability, into three regions in the electron concentration: in the low e/atom region, both the cubic $L1_2$ and the hexagonal $D0_{19}$ phases are more stable than the tetragonal $D0_{22}$ phase; for e/atom between $\sim$7.25 and 8.51, the cubic $L1_2$ phase has the lowest total energy; for e/atom above 8.57, the tetragonal $D0_{22}$ phase is the most stable phase. The stable hexagonal $D0_{19}$ phase emerges only in the e/atom region between 8.51 and 8.57. This is consistent with Ref. 4: $(Co,Ni)_3V$ corresponding to e/atom=8.54 has a 100% hexagonal (i.e., Ni_3Sn-type or $D0_{19}$) structure, while an increase in e/atom above 8.54 produces a change in the basic layer structure from T type to R type, which is related to the tetragonal $D0_{22}$ structure. In particular, in between e/atom=7.75 and 8.0, the total energy of the $L1_2$ phase reaches a minimum. Thus in this region, cubic $L1_2$ is most likely to be stabilized, which corresponds very well with experiments.[4] In the e/atom region between 8.0 and 8.51, the energy difference between $L1_2$ and $D0_{19}$ decreases; hence we might expect a mixture of both $L1_2$ and $D0_{19}$, and then a gradual structural transition from cubic $L1_2$ to hexagonal $D0_{19}$. This phenomenon is also observed experimentally.[4] Further, comparison between phase preference and e/atom in this region will be possible only after the study of the transition stacking of the hexagonal and the cubic structures (i.e., Al_3Pu structure, etc.) in this e/atom region is completed.

Finally, we inspected the DOS for the "constituent" compounds Ni_3V, Co_3V, and Fe_3V of the pseudobinary compounds $(Ni,Co,Fe)_3V$, and immediately found that e/atom is associated with the filling up of the bonding

TABLE IV. The total and partial (projected by angular momentum and site) DOS at E_F and number of electrons for Ni_3V in the $D0_{22}$ structure and Co_3V in the $L1_2$ structure. There are two different Ni sites (A and B) in Ni_3V [cf. Fig. 1(c)]. N and n represent the DOS at E_F and the number of electrons, respectively.

	Sites	N_s	N_p	N_d	N_{tot}	n_s	n_p	n_d	n_{tot}
$Ni_3V(D0_{22})$	Ni (A)	0.30	1.74	11.47	13.51	0.73	0.82	8.66	10.21
	Ni (B)	0.22	1.11	6.76	8.09	0.72	0.86	8.63	10.21
	V	0.19	0.97	13.06	14.22	0.49	0.60	3.28	4.37
$Co_3V(L1_2)$	Co	0.10	0.67	12.19	12.96	0.69	0.85	7.64	9.18
	V	0.12	0.33	2.43	2.88	0.51	0.62	3.32	4.45

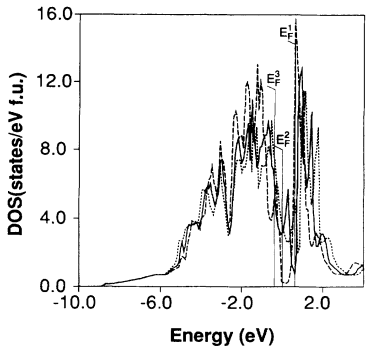

FIG. 6. Comparison of the total density of states for Ni_3V, Co_3V, and Fe_3V in $L1_2$ structure; the bottom of the density of states of Ni_3V (Fe_3V) has been shifted to coincide with that of Co_3V. Dashed, dotted, and solid lines denote Ni_3V, Fe_3V, and Co_3V, respectively. Here E_F^1, E_F^2, and E_F^3 denote the Fermi level of Ni_3V, Co_3V, and Fe_3V, respectively.

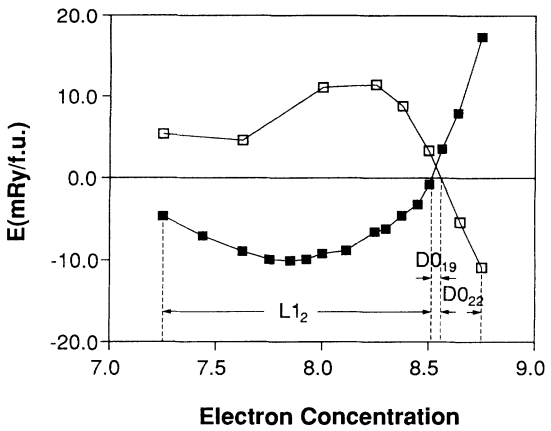

FIG. 7. Total-energy difference between $L1_2$ (or $D0_{22}$) and $D0_{19}$ structures vs electron concentration e/atom for the pseudobinary $(Ni,Co,Fe)_3V$ compounds. The total energy of the $D0_{19}$ structure is taken as reference energy. The open squares and solid squares represent the total energy of $D0_{22}$ and $L1_2$, respectively.

states. As stated above, the electronic structures for the Ni_3V, Co_3V, and Fe_3V compounds in the $L1_2$ structure (cf. Fig. 6) have a common feature, i.e., a deep valley (or pseudogap) that separates the d-d bonding and antibonding regions. The number of valence electrons accommodated in the bonding region is, surprisingly, nearly constant [33.83, 33.92, and 33.75 electrons (equivalently, e/atom=8.46, 8.48, and 8.44) for $L1_2$ Ni_3V, Co_3V, and Fe_3V, respectively]. In other words, for any of these $L1_2$ compounds, the bonding region can accommodate at most approximately 33.8 electrons (or e/atom$\sim$8.5). Similarly, the e/atom boundary (8.50, 8.49, and 8.53 for Ni_3V, Co_3V, and Fe_3V, respectively) is found for the hexagonal $D0_{19}$ structure. Any M_3V (M=Ni, Co, or Fe) compound possessing an electron concentration that exceeds the boundary value e/atom=8.5, has its extra valence electrons fall into the antibonding region; this destabilizes the cubic $L1_2$ (or hexagonal $D0_{19}$) structure and results in a phase transition to the $D0_{22}$ structure, which is more efficient in accommodating the valence electrons as compared to the $L1_2$ phase (cf. Sec. III A 3). This result is consistent with our model calculation and with Liu's finding[6] that for e/atom above 8.54 there is a change in the basic layer structure from T type to R type (the tetragonal $D0_{22}$ structure essentially consists of the stacking of the R layer).

ACKNOWLEDGMENTS

This work was supported by the Air Force Office of Scientific Research (Grant No. 88-0346) and by a computing grant at the Wright-Patterson Air Force Base Superconducting Center. The authors gratefully acknowledge helpful discussions with S. P. Tang and T. Hong.

[1] *Intermetallic Compounds,* edited by J. H. Westbrook (Wiley, New York, 1967).
[2] O. Izumi, Mater. Trans. JIM **9**, 627 (1989).
[3] R. L. Fleischer, D. M. Dimiduk, and H. A. Lipsitt, Ann. Rev. Mater. Sci. **19**, 231 (1989).
[4] C. T. Liu, in *Alloy Phase Stability,* edited by G. M. Stocks and A. Gonis (Kluwar Academic, Norwell, MA, 1989), p. 7.
[5] R. von Mises, Z. Angew. Math. Mech. **8**, 161 (1928).
[6] C. T. Liu and J. O. Stiegler, Science **226**, 636 (1984); C. T. Liu, Int. Metals Rev. **29**, 168 (1984); C. T. Liu and H. Inouye, Metall. Trans. A **10**, 1515 (1979); C. T. Liu, J. Nucl. Mater. **85&86**, 907 (1979).
[7] S. Pei, T. B. Massalski, W. M. Temmerman, P. A. Sterne, and G. Malcolm Stocks, Phys. Rev. B **39**, 5767 (1989).
[8] W. Kohn and L. J. Sham, Phys. Rev. **140**, A1133 (1965).
[9] O. K. Andersen, Phys. Rev. B **12**, 3060 (1975).
[10] U. von Barth and L. Hedin, J. Phys. C **5**, 1629 (1972); L. Hedin and S. Lundquivst, *ibid.* **4**, 2064 (1971).
[11] H. J. F. Jansen and A. J. Freeman, Phys. Rev. B **30**, 561 (1984).
[12] J. Rath and A. J. Freeman, Phys. Rev. B **11**, 2109 (1979).
[13] O. Kubaschewski, E. L. Evans, and C. B. Alcock, *Metallurgical Thermochemistry,* 4th ed. (Pergamon, Oxford, 1967).
[14] P. Villars and L. D. Calvert, *Pearson's Handbook of Crystallographic Data for Intermetallic Phases* (American Society for Metals, Metal Park, OH 1986).
[15] J. H. Xu, T. Oguchi, and A. J. Freeman, Phys. Rev. B **35**, 6940 (1987).
[16] *Smithells Metals Reference Book,* 6th ed., edited by E. A. Brandes (Butterworth, London, 1983).
[17] R. Hoffman, Rev. Mod. Phys. **60**, 601 (1988).
[18] J. H. Xu and A. J. Freeman, Phys. Rev. B **40**, 11 972 (1989).
[19] Y. Aoki, Y. Obi, and H. Komatsu, Z. Metallk. **70**, 436 (1979).
[20] E. T. Peters and L. E. Tanner, Trans. Met. Soc. AIME **233**,

2126 (1965).
[21]S. Saito, Acta Crystallogr. **12**, 500 (1959).
[22]C. D. Gelatt, A. R. Williams, and V. L. Moruzzi, Phys. Rev. B **27**, 2005 (1983).
[23]Y. Aoki and M. Yamamoto, Phys. Status Solidi A **33**, 625 (1976).
[24]*Binary Alloy Phase Diagrams,* edited by T. B. Massalski (American Society for Metals, Metal Park, OH, 1986).
[25]L. Vegard, Z. Phys. **5**, 17 (1921).